Acta Pharmaceutica Sinica B 2022;12(2):774−786

Chinese Pharmaceutical Association
Institute of Materia Medica, Chinese Academy of Medical Sciences

Acta Pharmaceutica Sinica B

www.elsevier.com/locate/apsb
www.sciencedirect.com

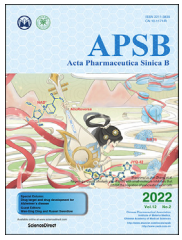

ORIGINAL ARTICLE

A novel PI3K inhibitor XH30 suppresses orthotopic glioblastoma and brain metastasis in mice models

Ming Ji[a,c,†], Dongjie Wang[b,†], Songwen Lin[a], Chunyang Wang[b], Ling Li[c], Zhihui Zhang[b], Jing Jin[a,c], Deyu Wu[a], Yi Dong[a], Heng Xu[a,*], Duo Lu[a,*], Xiaoguang Chen[a,b,*]

[a]*State Key Laboratory of Bioactive Substances and Functions of Natural Medicines, Institute of Materia Medica, Chinese Academy of Medical Sciences and Peking Union Medical College, Beijing 100050, China*
[b]*Beijing Key Laboratory of New Drug Mechanisms and Pharmacological Evaluation Study, Institute of Materia Medica, Chinese Academy of Medical Sciences and Peking Union Medical College, Beijing 100050, China*
[c]*Beijing Key Laboratory of Non-Clinical Drug Metabolism and PK/PD Study, Institute of Materia Medica, Chinese Academy of Medical Sciences and Peking Union Medical College, Beijing 100050, China*

Received 7 March 2021; received in revised form 21 April 2021; accepted 22 April 2021

KEY WORDS

Glioblastoma;
Brain metastasis;
PI3K−mTOR−AKT signaling pathway;
PI3K inhibitor;
IL-17A

Abstract Glioblastoma is carcinogenesis of glial cells in central nervous system and has the highest incidence among primary brain tumors. Brain metastasis, such as breast cancer and lung cancer, also leads to high mortality. The available medicines are limited due to blood−brain barrier. Abnormal activation of phosphatidylinositol 3-kinases (PI3K) signaling pathway is prevalent in glioblastoma and metastatic tumors. Here, we characterized a 2-amino-4-methylquinazoline derivative XH30 as a potent PI3K inhibitor with excellent anti-tumor activity against human glioblastoma. XH30 significantly repressed the proliferation of various brain cancer cells and decreased the phosphorylation of key proteins of PI3K signaling pathway, induced cell cycle arrest in G1 phase as well. Additionally, XH30 inhibited the migration of glioma cells and blocked the activation of PI3K pathway by interleukin-17A (IL-17A), which increased the migration of U87MG. Oral administration of XH30 significantly suppressed the tumor growth in both subcutaneous and orthotopic tumor models. XH30 also repressed tumor growth in brain metastasis models of lung cancers. Moreover, XH30 reduced IL-17A and its receptor IL-17RA *in vivo*. These results indicate that XH30 might be a potential therapeutic drug candidate for glioblastoma migration and brain metastasis.

*Corresponding authors.
E-mail addresses: xuheng@imm.ac.cn (Heng Xu), luduo@imm.ac.cn (Duo Lu), chxg@imm.ac.cn (Xiaoguang Chen).
[†]These authors made equal contributions to this work.
Peer review under responsibility of Chinese Pharmaceutical Association and Institute of Materia Medica, Chinese Academy of Medical Sciences.

https://doi.org/10.1016/j.apsb.2021.05.019

1. Introduction

Glioblastoma multiforme is growth of abnormal glial cells in brain tissues, accounts for the majority of primary tumors in central nervous systems and is approximately 80% of the malignant brain tumor[1,2]. Glioblastoma is characterized by rapid growth and extensive infiltration to neighboring brain tissues, which contributes to a high rate of mortality and recurrence[3]. Brain metastasis are the most common type of intracranial tumor[4−6]. Primary cancers including lung cancer, breast cancer, and melanoma are most likely to metastasize to the brain. About 10%−26% of patients who die from cancers will develop brain metastases[7,8]. Currently, temozolomide (TMZ) is the first-line chemotherapy drug for glioma treatment in clinical and its therapeutic effect depends on the MGMT methylation status[9,10]. Over the past decade, little progress has been made in improving the prognosis of patients with glioblastoma and brain metastasis[11]. Although immune checkpoint inhibitors such as PD-1 antibodies have been tested in glioblastoma, their efficacy is not satisfied[12−15]. Thus, there is an urgent need to develop more effective small molecules which can penetrate the blood−brain barrier for the treatment of glioblastoma.

The phosphatidylinositol 3-kinases (PI3Ks) are members of a unique and conserved family of intracellular lipid kinases that phosphorylate the 3′-hydroxyl group of phosphatidylinositol and phosphoinositides, which are grouped into three classes according to their structural characteristics, regulator effects and substrate specificity[16]. To date, the class 1 PI3Ks have been mostly characterized and demonstrated to take part in cell survival, metabolism, proliferation, and cytoskeletal organization[17−19]. As reported, there are many signaling pathways dysregulated in glioblastoma. Of those, the PI3K signaling pathway is the most frequently aberrant-activated[20,21]. There are approximately 88% of glioma with gene mutations which code the critical proteins in PI3K signaling pathway, such as amplification of *EGFR*, gain of function mutations including *PI3KCA*(p110α), *PI3KCB*(p110β) and *PIK3R1* (p85), or loss of *PTEN*[22−24]. Currently, investigations involving therapeutic targeting of the PI3K pathway result in the development of several distinct classes of drugs and more than 40 PI3K inhibitors enter the clinical trials. Among them, idelalisib, copanlisib and duvelisib have been approved by the FDA for clinically used in the treatment of patients with lymphoma[25,26], while alpelisib was indicated for breast cancers[27]. Indeed, there are several PI3K inhibitors that have been reported to be brain penetrable and reached various stages of clinical development for treating patients with glioblastoma, including NVP-BEZ235, XL765, GDC-0084 and PQR 309[28−30]. Development of small molecule inhibitors targeting the PI3K signaling pathway for the treatment of glioblastoma is of the broad perspective of application and essential clinical significance.

In this article, we reported a 2-amino-4-methylquinazoline derivative, XH30, as a potent PI3K inhibitor capable of penetrating the brain. XH30 showed potent anti-tumor activity in various brain tumor cells, especially in glioblastoma. It not only induced cell cycle arrest in G1 phase, but also inhibited glioblastoma migration. In both glioma xenograft and orthotopic mice models, XH30 could strongly suppress PI3K signaling pathway and inhibit tumor growth. In NCI-H460 brain orthotopic mice model which mimicked the brain metastasis of lung cancers, XH30 also repressed the tumor growth. Furthermore, we found that interleukin-17A (IL-17A) activated PI3K signaling pathway in both glioblastoma and lung cancer cell lines, while XH30 reversed this effect of IL-17A *in vitro* and repressed the IL-17A driven tumor invasion. These data indicated that XH30 might be a good choice for glioblastoma and brain metastasis of tumors.

2. Materials and methods

2.1. Reagents

XH30 was synthesized in-house as described previously[27]. PF-04691502 was purchased from Selleck Chemicals. Human IL-17A recombinant protein was from Peprotech.

2.2. Cell culture

The cell lines U87MG, U251, A172, Daoy, SH-SY-5Y, NCI-H460, NCI-H1975, NCI-H69 and NCI-H446 were obtained from Cell Resource Centre at the Institute of Medical Sciences, Peking Union Medical College (Beijing, China). U373 was kept by our laboratory. CTX and BV2 were from Prof. Dan Zhang (Peking Union Medical College, Beijing, China). All cell lines were cultured at 37 °C under 5% CO_2. Daoy, SH-SY-5Y, NCI-H460, NCI-H1975, NCI-H69 and NCI-H446 cells were in RPMI1640 medium. U87MG and U251 cells were in MEM medium with 1% NEAA. A172, CTX and BV2 cells were in DMEM medium. All the mediums were supplemented with 10% FBS, 100 units/mL penicillin and 100 mg/mL streptomycin. All cell lines were tested with mycoplasma detection kit (InvivoGen, Hong Kong, China).

2.3. Kinase assay

The compound was detected in Eurofins DiscoverX Corporation (San Diego, CA, USA) by KINOMEscan™ Profiling Service. For most assays, kinase-tagged T7 phage strains were grown in parallel in 24-well blocks in an *Escherichia coli* host derived from the BL21 strain. *E. coli* were grown to log-phase and infected with T7 phage from a frozen stock (multiplicity of infection = 0.4) and incubated with shaking at 32 °C until lysis (90−150 min). The lysates were centrifuged (6000×*g*) and filtered (0.2 μm) to remove cell debris. The remaining kinases were produced in HEK-293 cells and subsequently tagged with DNA for qPCR detection. Streptavidin-coated magnetic beads were treated with biotinylated small molecule ligands for 30 min at room temperature to generate affinity resins for kinase assays. The liganded beads were blocked with excess biotin and washed with blocking buffer [SeaBlock (Pierce), 1% BSA, 0.05% Tween 20, 1 mmol/L DTT] to remove unbound ligand and to reduce non-specific phage binding. Binding

reactions were assembled by combining kinases, liganded affinity beads, and test compounds in 1 × binding buffer (20% SeaBlock, 0.17 × PBS, 0.05% Tween 20, 6 mmol/L DTT). Test compounds were prepared as 40 × stocks in 100% DMSO and directly diluted into the assay. All reactions were performed in polypropylene 384-well plates in a final volume of 0.02 mL. The assay plates were incubated at room temperature with shaking for 1 h and the affinity beads were washed with wash buffer (1 × PBS, 0.05% Tween 20). The beads were then re-suspended in elution buffer (1 × PBS, 0.05% Tween 20, 0.5 μmol/L non-biotinylated affinity ligand) and incubated at room temperature with shaking for 30 min. The kinase concentration in the eluates was measured by qPCR.

2.4. Cell viability assay

Cell viability was assessed by 3-(4,5-dimethylthiazol-2-yl)-2,5-diphenyltetrazolium bromide (MTT; Sigma−Aldrich, St. Louis, MO, USA) or CCK8 assay as previously described[31]. Briefly, 1200−3500 cells/well were plated, and compounds were added after overnight adherence. After 72 h incubation at 37 °C under 5% CO_2, 0.5 mg/mL MTT were added and kept on incubating for 4 h. Then the supernatants were gently removed, and 100 μL DMSO was added to lyse the formazan, which was measured using a microplate reader (BioTek, Winooski, VT, USA) at 570 nm wavelength for MTT assay. For CCK8 assay, CCK8 was added and incubated for 3 h to detect at 450 nm. The value of half maximal inhibitory concentration (IC_{50}) was calculated by GraphPad Prism 8.0.1 (La Jolla, CA, USA).

2.5. Immunoblotting analysis

Cells or mice tumor tissues were collected and then lysed in a RIPA lysate buffer supplement with 1% protease inhibitor cocktail (Solarbio, Beijing, China) and 1% phosphatase inhibitor cocktail. Lysates were then centrifuged at 12,000×*g* for 20 min. Proteins were quantitated by the BCA assay (Solarbio). Equal amounts of proteins were resolved in an SDS-polyacrylamide gel and transferred to a polyvinylidene fluoride membrane (Millipore, Darmstadt, Germany). The membrane was washed twice with Tris-buffered saline containing 0.1% Tween-20 (TBST), blocked with TBST containing 5% non-fat milk for 30 min, and then incubated with primary antibody (1:1000−1:2000 dilution, all from Cell Signaling Technologies, Boston, MA, USA) in TBST at 4 °C overnight. After washing with TBST, the membrane was incubated with goat anti-rabbit or anti-mouse IgG−HRP conjugates (1:1000 dilution, both from Cell Signaling Technologies) for 1 h at room temperature. Bands were detected by enhanced chemiluminescence.

2.6. Cell cycle analysis

A flow cytometry assay was used to analyze the cell cycle distribution as previously reported[32]. Briefly, cells at logarithmic growth phase were plated into 6-well plates and incubated overnight. After treatment with the test substances for 24 h, the cells were harvested and fixed in cold 70% ethanol overnight at −20 °C, and then washed with PBS and stained with PI solution (20 mg/mL PI and 20 mg/mL RNaseA in PBS) for 30 min. The cell fluorescence was measured using BD FACS verse flow cytometer (BD Biosciences, Franklin Lakes, NJ, USA) and the cell cycle distribution was analyzed.

2.7. Transwell migration assay

Transwell migration assay was used to analyze the ability of tumor cells to invade as previously reported[33]. Briefly, thaw Matrigel at 4 °C and keep on the ice, then add 40 μL of diluted Matrigel to the upper chamber of each well. Allow the wells to sit without a cover until the Matrigel has completely dried onto the porous membranes. Trypsinize the experimental cells and collect the cells by centrifugation (200×*g*). Wash the cells one time by resuspending the cell pellets at a final concentration of 5×10^5 cells/mL in DMEM containing 0.1% BSA. Add 200 μL of the cell suspensions containing the analyte to the upper chamber of each coated insert. Add 600 μL of DMEM containing 20% FBS to the bottom well of the chamber. Incubate the plates containing the Transwells at 37 °C for 24 h. After 24 h, remove the liquid from the upper chamber and fix with methanol for 10 min, then stain with 1% crystal violet, wash and wipe off the cells that have not passed through the membrane, count and photograph under a microscope of 200 times, each group of three parallel holes.

2.8. Wound healing assay

The motility of the cells was evaluated by wound healing assay. NCI-H460 (NSCLC) and NCI-H446 (SCLC) were plated in 6-well plate at the density of 1.5×10^6 cells per well in DMEM and RPMI 1640 medium contained 10% FBS separately. After the cells reached confluence, a 10 μL pipette tip was used to generate a wound space and the cells were rinsed twice with sterile PBS to remove cell debris. Cells were incubated with or without 100 ng/mL human IL-17A recombinant protein, combined with 10 log-scaled concentration range of XH-30 from 5×10^{-7} to 5×10^{-9} mol/L, with medium contained 10% FBS. Consequently, photographs (magnification 10×) of the wounds were captured immediately after wound generation (0 h) and 24 h by inverted microscope.

2.9. Animal study

All procedures were approved by the Ethics Committee for Animal Experiments of the Institute of Materia Medica, Chinese Academy of Medical Sciences & Peking Union Medical College and conducted under the Guidelines for Animal Experiments of Peking Union Medical College (Beijing, China). The approval number is 00005214.

For subcutaneous mouse models, female BALB/c athymic nude mice (8−10 weeks old) were subcutaneously implanted with 1×10^7 U251 or U373 cells in 0.1 mL matrigel solution in the right flank of nude nice. After two weeks, tumor issue was harvested sterilely, and tumor cells were extracted from tissue homogenate. Then, the mice were implanted with 5×10^6 tumor cells each. Seven days later when the average tumor volumes reached to 100−300 mm^3, the mice were randomized and received treatment (Day 0). Mice was orally administrated with vehicle or XH30 at a dose of 2.5, 5 or 10 mg/kg dissolved in 0.5% CMC once daily for 21 days. There were six mice in each group. Tumor volume and body weight were monitored twice a week. Tumor volume was calculated using Eq. (1):

$$V = 1/2 \times L \times W^2 \quad (1)$$

where L is the maximum length of tumor, W is the maximum width of tumor. The mice were euthanized on Day 21 and the tumor issues were collected for immunoblotting or immunohistochemistry.

For U251, U87MG and NCI-H460 mice orthotopic models, eight to ten-week-old female BALB/c athymic nude mice (Vital River Laboratories, Beijing, China) were housed in standard facilities. For the intracranial tumor experiments, mice were anesthetized and stereotaxically injected with 2×10^5 U251, U87MG or NCI-H460 cells in 5 μL PBS, 2 mm right and 1 mm anterior to the bregma in the striatum at 3 mm depth with a 10 μL Hamilton syringe needle. After 3 days, mice bearing intracranial tumors were randomized to orally receive the vehicle, TMZ or XH30 dissolved in 0.5% CMC. Animal magnetic resonance imaging (MRI) scanner (Pharma Scan 70/16 US, Bruker, Germany) was used to observe the intracranial tumor development. The parameters for MRI were as follows: a T2_TurboRARE, with TR/TE = 5000/40, 6 averages, 20 × 20 field-of-view, and 0.5 mm slice thickness. The tumor volume based on MRI was calculated as Eq. (2):

$$V = L \times W \times T \quad (2)$$

where L is the maximum length of tumor, W is the maximum width perpendicular to L and T is the thickness of the tumor slice (0.5 mm).

2.10. *Immunohistochemistry*

Five-micrometer sections of formalin-fixed paraffin-embedded samples were de-paraffinized and rehydrated, antigen retrieval was performed by microwave heating in citrate buffer (pH 6.0) for 30 min, and endogenous peroxidase activity was blocked with 3% H_2O_2. Then, sections were incubated at room temperature with goat serum for 2 h and then at 4 °C with the indicated antibodies for overnight. Sections were further processed with HRP-conjugated second

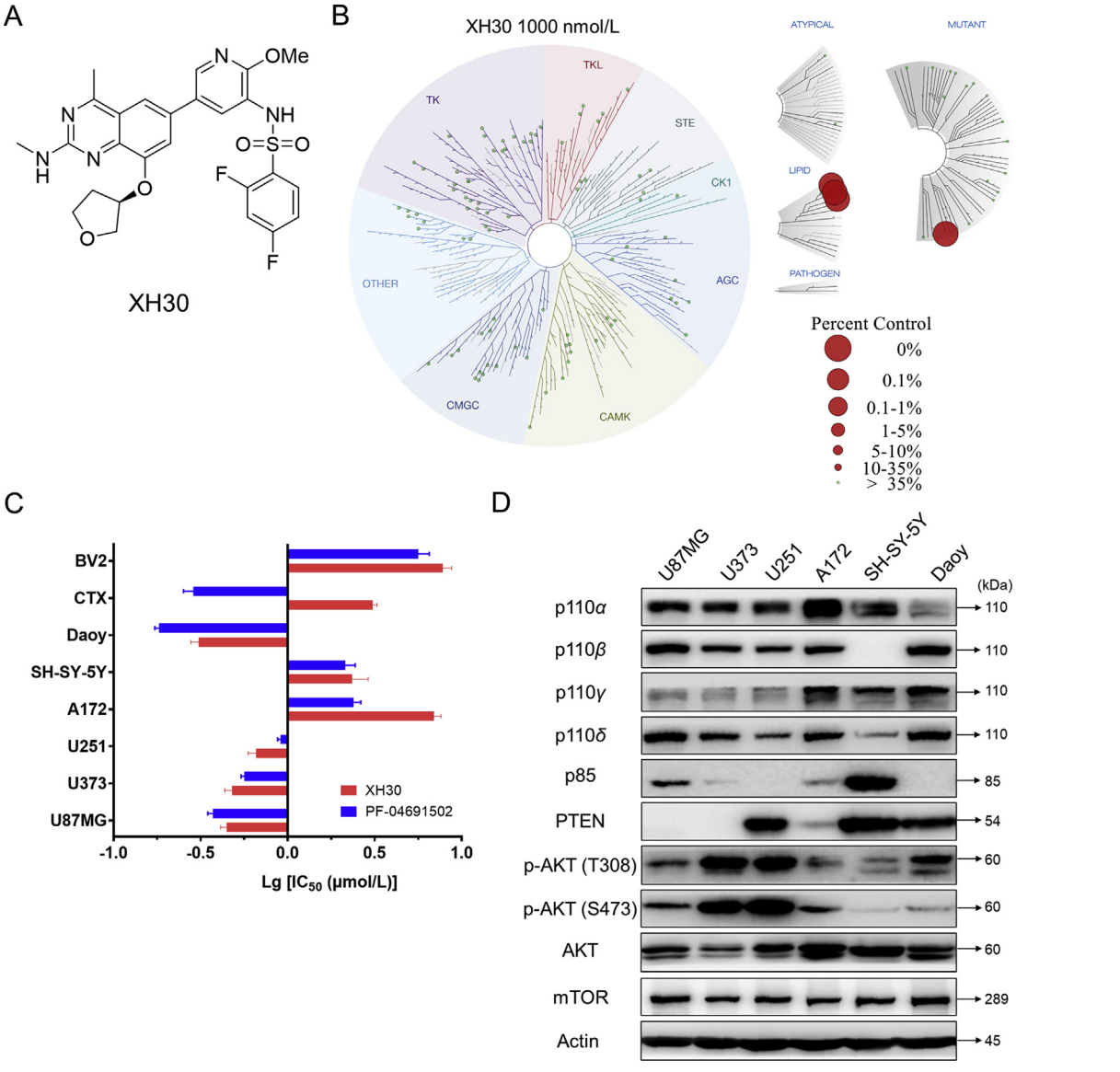

Figure 1 XH30 inhibited cell proliferation in various brain tumor cell lines. (A) Chemical structure of XH30. (B) Kinase interaction maps of XH30. (C) Relative sensitivity of brain tumor cells to XH30. Cell inhibition was assessed by MTT assay after 72 h incubation with the indicated compounds. The IC_{50} values are presented as mean ± SD, $n = 3$. (D) The expression pattern of PI3K signaling pathway in various brain tumor cells. The cells were then lysed and examined on crucial proteins of PI3K pathway signaling by immunoblotting.

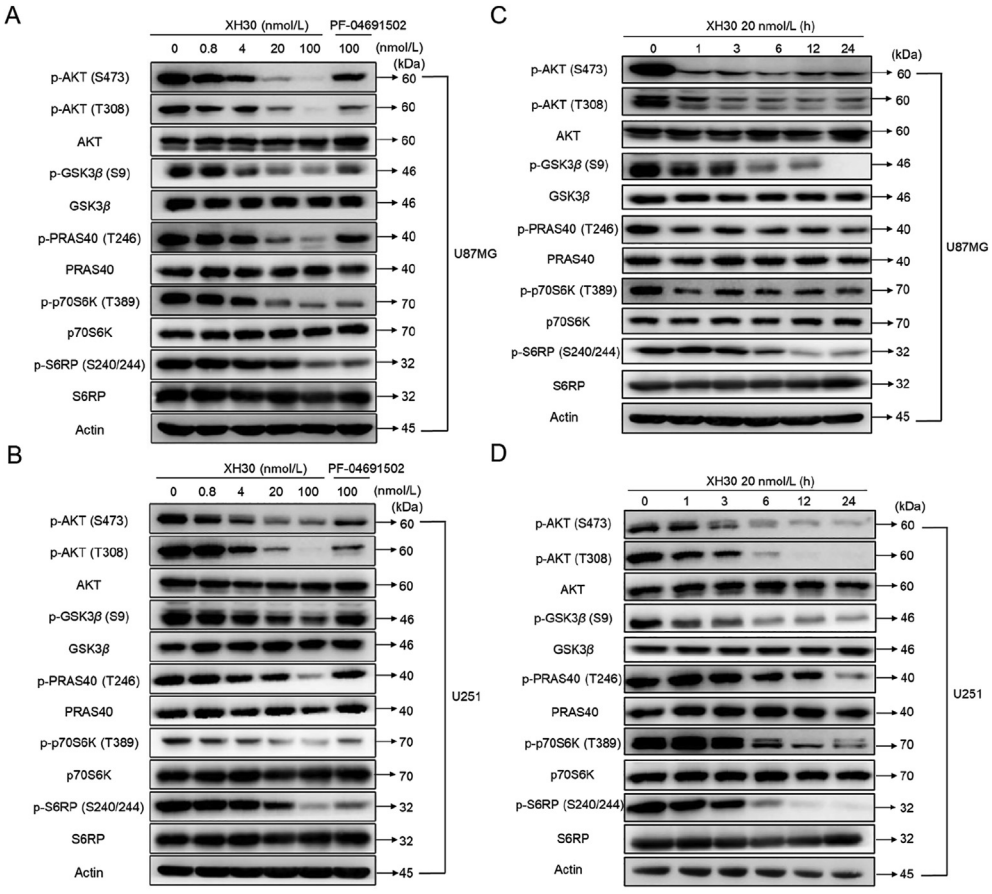

Figure 2 XH30 suppressed PI3K signaling pathway in glioblastoma cells. (A) XH30 dose-dependently inhibits PI3K pathway signaling in U87MG cells. The cells were incubated with XH30 at indicated concentrations (0.8, 4, 20, and 100 nmol/L) or PF-04691502 (100 nmol/L) for 3 h. (B) XH30 dose-dependently inhibits PI3K pathway signaling in U251 cells. The cells were incubated with XH30 at indicated concentrations (0.8, 4, 20, and 100 nmol/L) or PF-04691502 (100 nmol/L) for 3 h. (C) XH30 time-dependently inhibits PI3K pathway signaling in U87MG cells. The cells were incubated with XH30 (20 nmol/L) at indicated time points. (D) XH30 time-dependently inhibits PI3K pathway signaling in U251 cells. The cells were incubated with XH30 (20 nmol/L) at indicated time points. All cells were then lysed and effects of compounds on PI3K pathway signaling assessed by immunoblotting.

antibody and developed with 3,3-diaminobenzidine. Finally, visualization was performed with DAB reagent kit and hematoxylin. Images were obtained from an Olympus IX70 microscope (Tokyo, Japan).

2.11. *Statistical analysis*

Most statistical analyses were performed utilizing GraphPad Prism 8.0.1 (La Jolla, CA, USA) and the significance levels were evaluated using ANOVA analysis. Three asterisks (***), two asterisks (**), one asterisk (*) and no asterisk indicated in figures and tables represent $P < 0.001$, $0.001 < P < 0.01$, $0.01 < P < 0.05$ and $P > 0.05$, respectively.

3. Results

3.1. *XH30 showed strong anti-proliferation activities in various brain cancer cell lines*

XH30 is designed as a selective PI3K inhibitor, with a molecular weight of 557.6 (Fig. 1A). Kinase binding assay revealed XH30 specific targeted class 1 PI3Ks (Fig. 1B and Supporting Information Fig. S1A). In our previous study, XH30 has exhibited potent anti-tumor activities in various cancers[34]. It could inhibit U87MG growth *in vitro* and *in vivo* with blood−brain barrier penetrant capacity. This observation drove us to explore if XH30 has comprehensive anti-tumor activities in various brain cancers. Here, the growth inhibition effects of XH30 on six brain tumor cells were detected by MTT assay (Fig. 1C and Fig. S1B). The results show that the inhibitory activity of XH30 on brain tumors was comparable to that of PF04691502, a potent PI3K inhibitor as positive control. Among them, the inhibitory activities of XH30 in glioblastoma cell lines U87MG, U373, U251 and medulloblastoma cell line Daoy were much more potent than in glioblastoma cell line A172 and neuroblastoma cell line SH-SY-5Y cells. This may attribute to aberrant activated PI3K pathway in these cells with high level of phosphorylated AKT, *PTEN* deficiency or *PI3K* gene mutation, compared to A172 and SH-SY-5Y (Fig. 1D). U87MG cell is a *PTEN*-null cell, and *PIK3CB* was mutated in Daoy cells. Meanwhile, the effects of XH30 and PF04691502 on the growth of rat normal astrocyte CTX and mouse microglia BV2 were also examined. It was found that the IC_{50} values of XH30 on normal

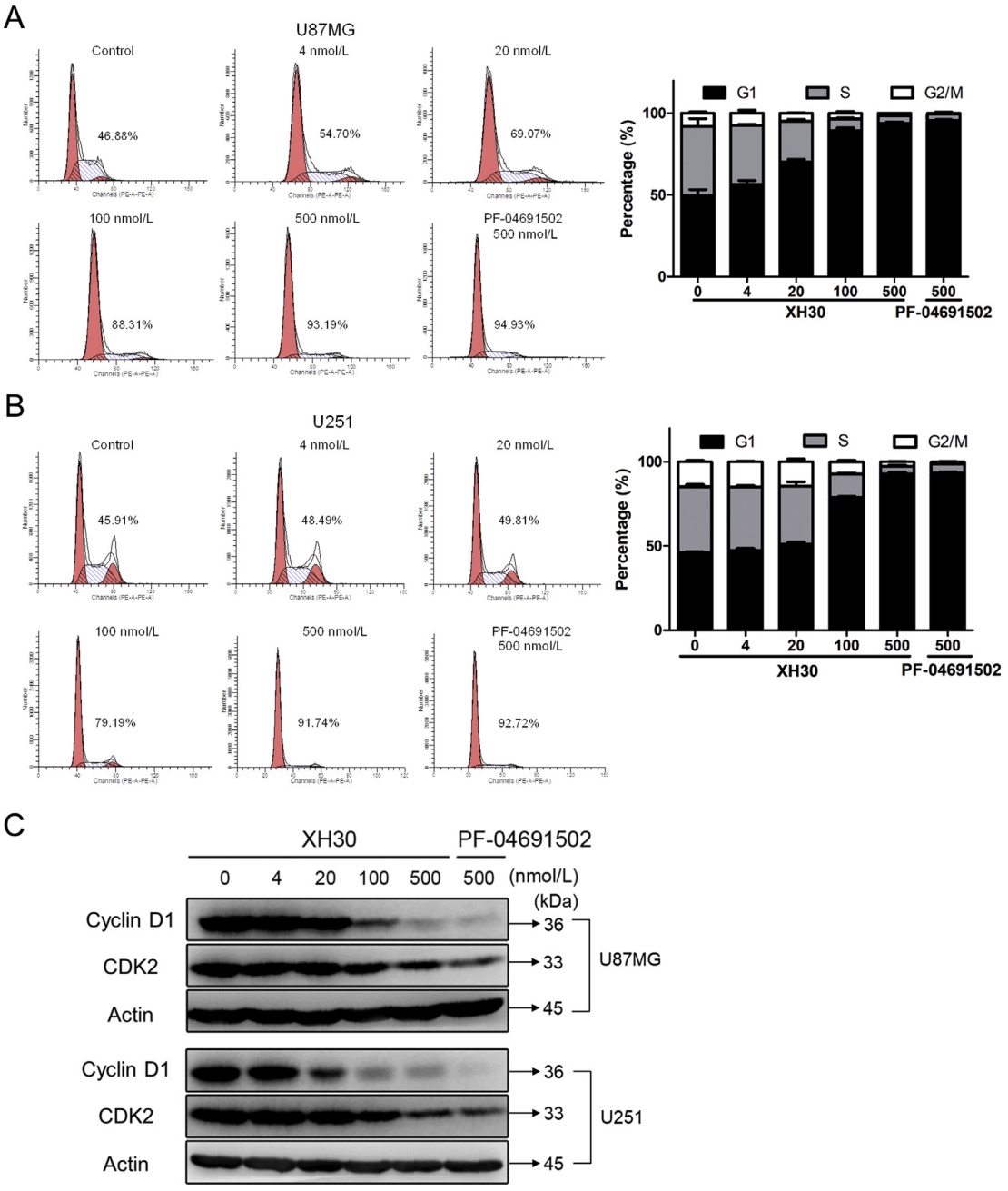

Figure 3 XH30 induced G1 cell-cycle arrest in glioblastoma cells. (A) XH30 induced U87MG cell cycle arrest in G1 phase. Exposure to various concentrations of XH30 at indicated concentrations (4, 20, 100 and 500 nmol/L) or PF-04691502 (500 nmol/L) for 24 h. The cells were stained with PI for flow cytometry analysis, $n = 3$. (B) XH30 induced U251 cell cycle arrest in G1 phase. Exposure to various concentrations of XH30 at indicated concentrations (4, 20, 100 and 500 nmol/L) or PF-04691502 (500 nmol/L) for 24 h. The cells were stained with PI for flow cytometry analysis, $n = 3$. (C) XH30 downregulated the markers of G1 cell-cycle. The protein levels of cyclin D1 and CDK2 were detected *via* immunoblotting in both U87MG and U251 cells exposure to XH30 for 24 h.

cells were significantly higher than that of PF04691502, indicating that XH30 may have low toxicity in brain.

3.2. *XH30 dose- and time-dependently blocked PI3K signaling pathway in glioblastoma cells*

As XH30 exhibited robust anti-tumor activity in central nervous glioblastoma cells, we further investigated its effect on PI3K signaling pathway. U87MG and U251 were exposed to XH30 with various concentrations or PF-04691502 at the dose of 100 nmol/L for 12 h. As shown in Fig. 2A, XH30 dose-dependently inhibited phosphorylation of AKT in U87MG cells. The phosphorylation level of AKT was almost completely inhibited by XH30 at 100 nmol/L, and the phosphorylation inhibition of AKT downstream effector molecules GSK3β and PRAS40 was consistent with the effect on AKT. In addition, XH30 also showed significant inhibition of the substrate p70S6K of mTORC1 and the substrate S6RP of p70S6K. Consistently, 100 nmol/L of XH30 strongly inhibited the phosphorylation of signaling pathway proteins in U251 cells (Fig. 2B). The inhibitory

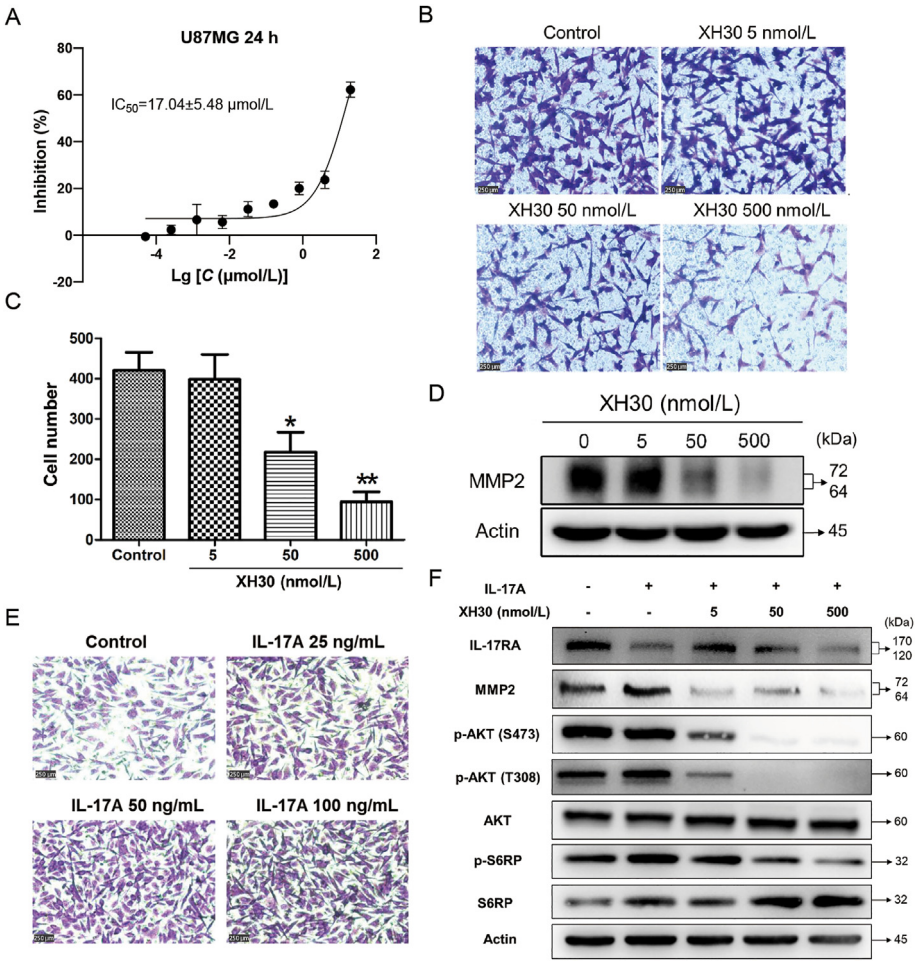

Figure 4 XH30 inhibits glioblastoma migration. (A) The IC_{50} value of XH30 in U87MG cells at 24 h. Data are presented as mean ± SD, $n = 3$. (B) Transwell migration assay in U87MG. The cells were exposed to various concentrations of XH30 (5, 50 and 500 nmol/L) for 24 h. 1% crystal violet staining, scale bar: 250 μm. (C) The count of migrated cells. Data are presented as mean ± SD, $n = 3$. ANOVA analysis, $^{*}P < 0.05$, $^{**}P < 0.01$, compared to control. (D) XH30 downregulated MMP2 expression. U87MG cells were exposed to XH30 for 24 h, then harvested for immunoblotting. (E) IL-17A increased the migration of U87MG cells. The cells were exposed to indicated concentrations of IL-17A for 24 h. 1% crystal violet staining, scale bar: 250 μm. (F) XH30 blocked the activation of PI3K/AKT pathway by IL-17. U87MG cells were incubated with XH30 at indicated concentrations (5, 50 and 500 nmol/L) in the presence or absence of 100 ng/mL hIL-17A for 24 h.

activity was much more potent than the positive control PF-04691502 at the same concentration. Furthermore, U87MG and U251 cells were treated with XH30 at the concentration of 20 nmol/L for different timepoints. XH30 rapidly inhibited phosphorylated levels of AKT at 1 h and this inhibitory effect maintained to 24 h (Fig. 2C). At the same time, the phosphorylation levels of GSK3β, pRAS40 and p70S6K also decreased. The expression of phosphorylation of S6RP began to reduce at 6 h. U251 cells exposure to XH30 exhibited inhibition of phosphorylation of AKT and its downstream proteins as well. The phosphorylation levels of pRAS40, p70S6K and S6RP downregulated from 6 h (Fig. 2D).

3.3. *XH30-mediated glioblastoma cell growth inhibition is associated with G1 cell-cycle arrest*

PI3K signaling pathway plays a key role in cell cycle progression. As shown in Fig. 3A, after incubating with XH30 at the concentration of 4, 20, 100 and 500 nmol/L for 24 h, U87MG cells were arrested at G1 phase from 46.88% up to 93.19%. Similar results were observed in U251 cells (Fig. 3B), the percentage of U251 cells in the G1 phase is 45.91% up to 91.74%. Immunoblotting was used to detect the effector proteins cyclin D1 and CDK2, both of which are key proteins in the G1 phase. The expression of cyclin D1 and CDK2 decreased in a dose-dependent manner after 24 h of U87MG and U251 cells (Fig. 3C). At the same dose, the inhibition of XH30 was comparable to that of PF-04691502. This indicates that XH30 inhibits the expression of cyclin D1 and CDK2 proteins, resulting in G1 arrest in glioma cells.

3.4. *XH30 inhibits the migration of glioblastoma*

PI3K signaling pathway is also involved in tumor migration and invasion. To investigate the effect of XH30 on glioma cell invasion, we employed transwell migration assay in U87MG cell. We firstly tested the survival of cells exposed to XH30 for 24 h. Fig. 4A shows that The IC_{50} value of XH30 was 17.04 μmol/L, and the inhibition rate is less than 20% at the concentration of 500 nmol/L. Thus, the maximum concentration of 500 nmol/L was selected for migration assay. After 24 h of treatment, the

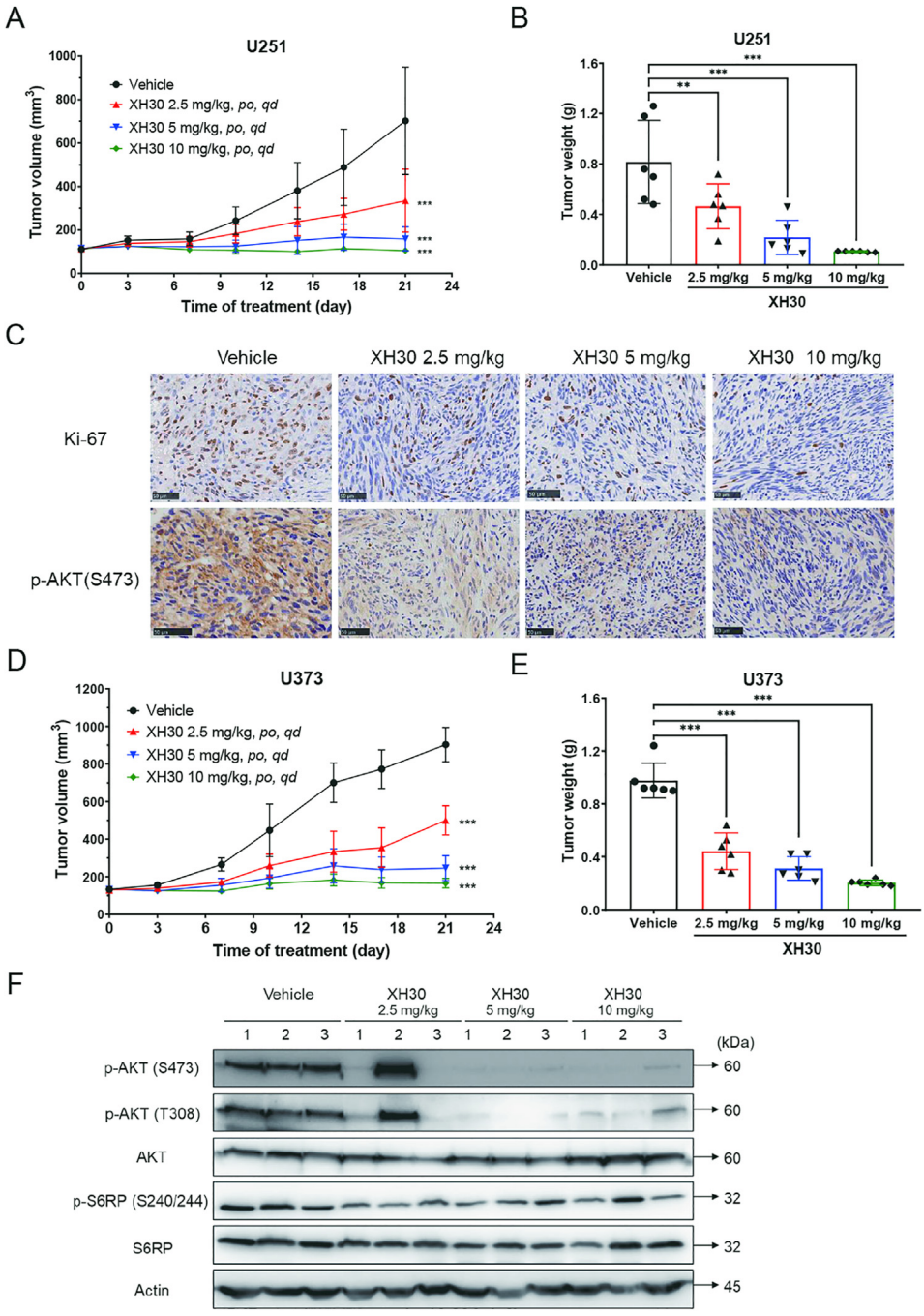

Figure 5 XH30 repressed glioblastoma growth in subcutaneous xenograft models. (A) The tumor growth curve in U251 xenograft mice model. Data are presented as mean ± SD, $n = 6$. ANOVA analysis, $^{***}P < 0.001$, compared to vehicle group. (B) The tumor weight in U251 xenograft mice model. ANOVA analysis, $^{**}P < 0.01$, $^{***}P < 0.001$, compared to vehicle group. Data are presented as mean ± SD, $n = 6$. (C) Histological analysis of tumor issues in U251 xenograft model. Ki67 and p-AKT (473) staining. Scale bar: 50 μm. (D) The tumor growth curve in U373 xenograft mice model. Data are presented as mean ± SD, $n = 6$. ANOVA analysis, $^{***}P < 0.001$, compared to vehicle group. (E) The tumor weight in U373 xenograft mice model. Data are presented as mean ± SD, $n = 6$. ANOVA analysis, $^{***}P < 0.001$, compared to vehicle group. (F) XH30 inhibited PI3K signaling pathway in tumor tissue from U373 xenograft mice model.

number of cells passing through the transwell chamber dose-dependently decreased in XH30 groups (Fig. 4B and C). As shown in Fig. 4D, XH30 significantly reduced the expression of MMP2 protein at the concentration of 5, 50, and 500 nmol/L, but not changed the expression of epithelial−mesenchymal transition (EMT) markers and other MMPs (Supporting Information Fig. S2A and S2D).

It was reported that IL-17A promoted tumor migration and invasion in glioblastoma *via* activation of PI3K/AKT signaling pathway[35]. Here, we found that IL-17A did not enhance the

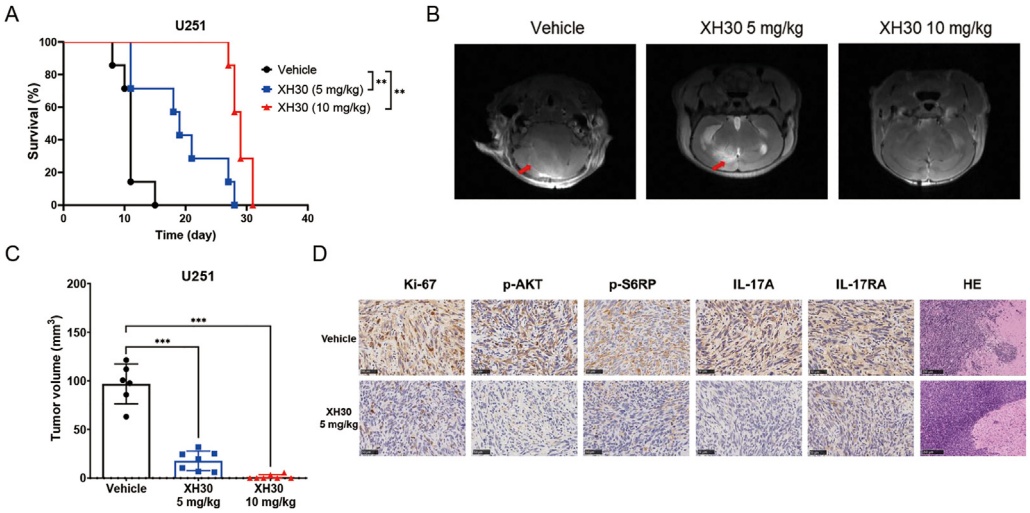

Figure 6 XH30 repressed glioblastoma growth in glioblastoma orthotopic models. (A) Life survival curve of XH30 in U251 orthotopic model. The mice were orally administered by vehicle or XH30 for ten days, and then monitored. $n = 6$, ANOVA analysis, $^{**}P < 0.01$, compared to vehicle group. (B) Representative MRI images from U251 orthotopic model on Day 11. Red arrow indicated tumor. (C) The tumor volumes in U251 orthotopic model on Day 11. $n = 6$, ANOVA analysis, $^{***}P < 0.001$, compared to vehicle group. (D) Histological analysis of tumor issues in mouse brain of U251 orthotopic model on Day 11. Ki-67, p-AKT (S473), p-S6RP (S240/S244), IL-17A and IL-17RA staining, scale bar: 50 μm. HE staining, scale bar: 250 μm.

proliferation of U87MG cells (Fig. S2B), but indeed forced the migration of U87MG cells (Fig. 4E). This was not related to increase the expression of EMT markers or MMPs excluding MMP2 (Fig. S2C and S2D). IL-17A activated the PI3K/AKT pathway, especially elevated the phosphorylation level of AKT at T308, and upregulated the expression of MMP2, while XH30 blocked the activation of PI3K/AKT by IL-17A and downregulated MMP2 in U87MG cells (Fig. 4F). Taken together, these data indicate that XH30 could inhibit the migration of glioma.

3.5. *XH30 inhibited tumor growth in both subcutaneous and orthotopic xenograft mice models*

To confirm the effect of XH30 against glioblastoma *in vivo*, we investigated the anti-tumor activities of XH30 in mice xenograft models. As shown in Fig. 5A, XH30 significantly repressed subcutaneous tumor growth of U251 in a dose-dependent manner with *P*-value less than 0.001. The tumor growth inhibition of tumor weight for XH30 were 43.1% (2.5 mg/kg), 73.3% (5 mg/kg) and 86.9% (10 mg/kg), compared to vehicle group (Fig. 5B, Supporting Information Fig. S3A and S3B). Histological data (Fig. 5C) show that ki67 was reduced after XH30 treatment, which indicated that XH30 inhibited tumor growth. The phosphorylation level of AKT at S473 was undoubtedly decreased after XH30 treatment compared to vehicle group. In another mice model of U373 xenograft model, XH30 also suppressed the tumor growth in dose-dependent manner (Fig. 5D and E, Supporting Information Fig. S4A and S4B). The immunoblotting results show that the crucial proteins of PI3K signaling pathway were downregulated in those tumor tissues exposed to XH30 (Fig. 5F).

To further assess the anti-tumor activity of XH30 in glioblastoma *in vivo*, U251 orthotopic xenograft model was employed. During the experiment, mice were given ascending doses of XH30. The life survival was monitored, and intracranial tumors were observed by MRI on Day 11. As shown in Fig. 6A, XH30 significantly extended the survival curve of mice with *P*-value less than 0.01, compared to vehicle group. Consistently, the tumor volumes in both 5 and 10 mg/kg groups of XH30 were much smaller compared to vehicle group (Fig. 6B and C and Supporting Information Fig. S5A). Two moribund mice in vehicle group and one moribund mouse in XH30 group at the dose of 5 mg/kg were deposited for immunobiological analysis. Histological results indicate a remarkable decline of phosphorylated levels of AKT at S473, S6RP at S240/244 and ki67 expression in XH30 groups compared to vehicle group. Interestingly, the expression of IL-17A and IL-17RA was also decreased in XH30 group. HE results also indicate that XH30 effectively inhibited glioblastoma invasion. Additionally, XH30 was repeated in U87MG orthotopic xenograft model (Supporting Information Fig. S6A and S6B). The tumor samples were also collected for histological test. Histological results indicate a remarkable decline of phosphorylated levels of AKT at 473 site and ki67 expression in XH30 groups compared to vehicle group (Fig. S6C). HE results show the similar results as the one in U251 model. These results display the outstanding capability of XH30 against glioblastoma.

3.6. *XH30 repressed tumor growth in brain metastasis of lung cancer*

As XH30 inhibited glioblastoma growth *in vitro* and *in vivo*, we explored if XH30 also exhibited good anti-tumor activities against metastatic tumor. Lung cancers were of high brain metastatic ratio, especially small cell lung cancer. Literature has revealed that IL-17A was involved in brain metastasis of lung cancer[36]. Thus, we investigated if XH30 could reversed the roles of IL-17A on lung cancer cells. We firstly assessed the inhibitory effect of XH30 in both SCLC and NSCLC cell lines. As shown in Fig. 7A, XH30 could inhibit cell proliferation of NCI-H460, NCI-H1975, NCI-H441 and NCI-H69. These cells were then tested exposed to XH30 in the presence of IL-17A. As shown in Fig. 7B and C, IL-17A activated the PI3K/AKT signaling pathway in these cells, while the elevated phosphorylation levels of AKT and S6RP by

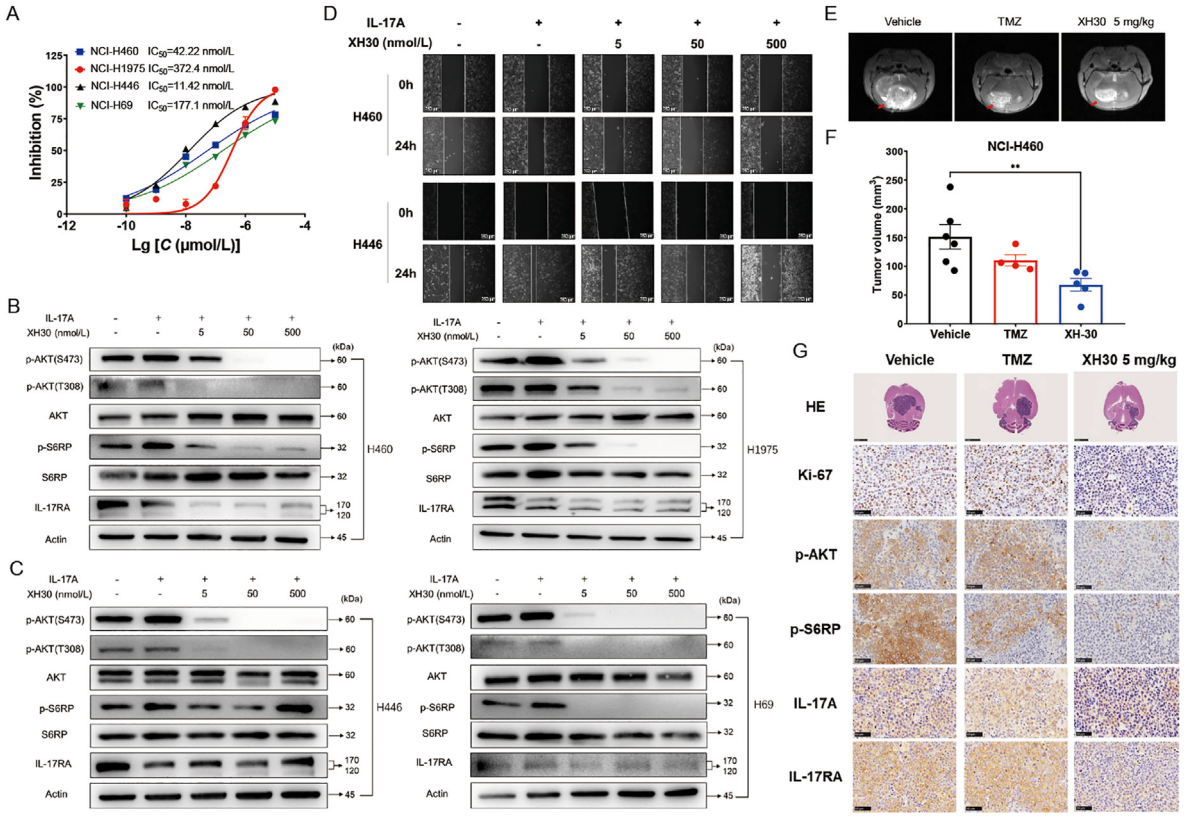

Figure 7 XH30 repressed tumor growth in brain metastasis of lung cancer. (A) The IC_{50} values of XH30 in various lung cancer cell lines for 72 h. Data are presented as mean ± SD, $n = 3$. (B) and (C) XH30 dose-dependently inhibits IL-17A activated PI3K pathway signaling in various lung cancer cell lines. The cells were incubated with XH30 at indicated concentrations (5, 50 and 500 nmol/L) in the presence of 100 ng/mL hIL-17A for 24 h. (D) Wound healing assay of NCI-H460 and NCI-H446 cells by XH30 in the presence of IL-17A. Wound space was captured at 0 and 24 h post scratching by inverted microscope (scale bar: 250 μm). Representative images are shown. (E) Representative MRI images from NCI-H460 brain orthotopic model. Red arrow indicated tumor. (F) The tumor volumes in NCI-H460 brain orthotopic model. Data are presented as mean ± SD. ANOVA analysis, $^{**}P < 0.01$, compared to vehicle group. (G) Histological analysis of tumor issues in mouse brain of NCI-H460 orthotopic model. Ki-67, p-AKT (S473), p-S6RP (S240/S244), IL-17A and IL-17RA staining, scale bar: 50 μm. HE staining, scale bar: 250 μm.

IL-17A were reduced exposed to XH30. XH30 also downregulated IL-17RA. Moreover, IL-17A enhanced the invasion of NCI-H460 and NCI-H441. XH30 blocked the invasion induced by IL-17A in a dose dependent manner (Fig. 7D).

According to the results *in vitro*, we employed lung cancer xenograft model which NCI-H460 cells were implanted in mice brain to mimic brain metastasis. After administration of XH30 for 8 days, the tumors were viewed by MRI. XH30 indeed significantly repressed NCI-H460 tumor growth in brain compared to vehicle group (Fig. 7E and F and Supporting Information Fig. S7A). This effect is much better than TMZ. The histological data show that the phosphorylation levels of AKT and S6RP and the expression of ki67 in XH30 groups were decreased compared to vehicle group (Fig. 7G). Additionally, the expressions of IL-17A and IL-17RA were also reduced in XH30 group at the dose of 5 mg/kg. Taken together, these data indicate that as a brain penetrating PI3K inhibitor, XH30 also repressed the brain metastasis of lung cancers.

4. Discussion

PI3Ks are a family of lipid kinases that integrate signals from growth factors, cytokines and other environmental cues, translating them into intracellular signals that regulate multiple signaling pathways[37]. Activating alterations in PI3K are found frequently in a variety of cancers, making this class of enzymes a prime drug target for anti-cancer therapy[38,39]. In 2014, the first-in-class PI3K inhibitor idelalisib was approved by the US FDA for the treatment of patients with follicular lymphoma and small lymphocytic lymphoma[40], which has brought hope to the effective cancer treatment by inhibiting the PI3K signaling pathway. More recently, alepelisib was approved for breast cancer, extending the indications for PI3K inhibitors to solid tumors[27]. While more than 40 structurally distinct PI3K inhibitors have entered clinical trials, only a few of them are reported to be brain penetrant and can be appropriately tested for brain cancers[24,25,30,41–43]. The brain–blood barrier limits over 90% small molecules to access the brain and discovery of PI3K inhibitors capable of penetrating the brain requires the rational design[44].

Previous study has showed that XH30 potently inhibited class I PI3K isoforms[34]. Pharmacokinetics data showed XH30 was able to cross the blood–brain barrier with the brain concentration significantly higher than the kinase and cellular IC_{50} values. Here, we studied the growth inhibition of XH30 against different kinds of brain tumor and lung cancer cell lines together with normal glial cells by MTT or CCK8 assays. The results showed that XH30 showed strong growth inhibitory activity against glioblastoma cells U87MG, U373, U251, and medulloblastoma

cell Daoy, compared to glioblastoma cell A172 and neuroblasts SH-SY-5Y. We detected the expression of key proteins in the PI3K pathway in the above brain cancer cell lines. It was found that the AKT phosphorylation levels were low in both A172 and SH-SY-5Y cells compared to U251 and U373, suggesting that anti-tumor activity of XH30 attributed to high levels of activated AKT. Besides, mutation or loss of genes referred to *PI3K* function could overactivate this pathway. That is why XH30 showed strong activities in U87MG and Daoy cells compared to A172 and SH-SY-5Y cells. The activity was also observed in lung cancer cells NCI-H460, NCI-H1975, NCI-H446 and NCI-H69. In addition, the IC_{50} of XH30 is 10^{-6} mol/L on normal glial cells BV2 and CTX, while the IC_{50} of PF04691502 is 10^{-7} mol/L on astrocytes CTX, which suggested the less toxic, higher safety profile of XH30 on normal cells.

PI3K pathway is closely related to cell cycle progression[45]. We performed PI flow cytometry experiments in U87MG and U251 cells. The results show that XH30 induced G1 arrest in a dose-dependent manner. And decreased the expression of the G1-related proteins cyclin D1 and CDK2, downstream of the PI3K pathway. It showed that XH30 can achieve anti-tumor effect through cycle arrest. Additionally, brain tumors generally do not metastasize, but glioblastoma has a strong invasive effect on surrounding tissues[46]. It has been reported in the literature that the PI3K pathway is involved in the regulation of cell invasion and migration[46–48]. We found that XH30 indeed inhibited U87MG migration *in vitro* and downregulated MMP2 expression, but had no effect on EMT. The PI3K pathway-related proteins in U87MG and U251 were significantly reduced exposed to XH30. And XH30 also dampened IL-17A-promoted NCI-H460 and NCI-H446 invasion *in vitro*. This trigger us to further test the anti-tumor activities of XH30 against glioblastoma and brain metastasis of lung cancer *in vivo*.

In vivo, both subcutaneous and orthotopic glioblastoma models were performed to assess the anti-tumor activity of XH30. We firstly evaluate the anti-tumor activity in U251 and U373 xenograft models. As expected, XH30 dose-dependently suppressed tumor growth in both models. Both histological and immunoblotting results show the PI3K signaling pathway was significantly inhibited by XH30. All these data support the anti-tumor activity of XH30 *in vivo*. However, due to brain–blood barrier, these subcutaneous models can not reflect the actual effect of XH30 against glioblastoma. Thus, we employed U251 and repeated U87MG orthotopic glioblastoma models to confirm this observation and access the effect of XH30 in PI3K signaling pathway. Consistently with subcutaneous models, XH30 significantly inhibited tumor growth in a dose-dependent manner in both U251 and U87MG orthotopic model and the immunohistochemistry results show that XH30 could significantly decrease the ki67 positive expression and blocked PI3K signaling pathway in tumor tissues. The body weight changes in XH30 groups were acceptable in all these three models (Figs. S3B, S4C, S5B and S6D). However, the counts of peripheral total white blood cells, lymphocytes and neutrophils were decreased in XH30 group at the dose of 5 mg/kg (Fig. S6E). This may attribute to the inhibition of PI3K delta and gamma isoforms by XH30. Additionally, PI3K alpha isoform related blood glucose in mice was elevated at the dose of 10 mg/kg XH30 (Figs. S3D and S4D). Overall, the mice were well tolerated in exposure to XH30.

IL-17A plays important roles in various inflammatory diseases and cancers including several extracranial and some intracranial tumors[36,49,50]. The IL-17A expression levels were positively correlated with the WHO pathological classification of GBM and associated with the progression and brain metastasis of lung carcinoma[35]. IL-17A has been shown to promote glioblastoma development by enhancing glioma cell migration and invasion *via* activation of PI3K/AKT signaling pathway[51]. Here, we found that IL-17A also activated PI3K pathway in both SCLC and NSCLC cells. Blockage of PI3K pathway by XH30 reversed IL-17 driven PI3K activation. *In vivo*, XH30 could repressed orthotropic lung cancer growth in brain (Fig. S7) and downregulated IL-17A and its receptor IL-17RA expression. This indicates that XH30 might be a choice for brain metastasis by reducing IL-17A. However, this model had some limitations. Xenograft models could not exhibit the pathological progression of brain metastasis and evaluated the complete roles of IL-17A in brain metastasis as the mice was athymic nude. Intriguingly, without Th17 cells contribution, IL-17A was still detected in cancer tissues in brain. This trigger us to explore the other IL-17A producing cells and find potential mechanism how XH30 reduces IL-17A expression in future.

5. Conclusions

A potent PI3K inhibitor XH30 has been characterized to exhibit robust antitumor activities and is expected to be developed into a therapeutic brain tumor drug.

Acknowledgement

This work was supported by the CAMS Innovation Fund (2016-I2M-3-008, China), The Drug Innovation Major Project (2018ZX09711001-003-011 and 2018ZX09711001-005-017, China), and the Non-Profit Central Research Institute Fund of Chinese Academy of Medical Sciences (Grant 2018PT35003, China).

Author contributions

Ming Ji, Dongjie Wang and Chunyang Wang designed the experiments. Ming Ji, Dongjie Wang, Chunyang Wang and Ling Li conducted all the experiments. Songwen Lin, Deyu Wu and Yi Dong synthesized the compound. Zhihui Zhang, Dongjie Wang and Ling Li analyzed the data. Jing Jin, Yi Dong and Ming Ji obtained the funding. Ming Ji and Ling Li drafted the manuscript. Heng Xu, Duo Lu and Xiaoguang Chen reviewed and edited the manuscript, and supervised the whole study as well. All authors approved the final version of the manuscript.

Conflicts of interest

The authors report no conflict of interest.

Appendix A. Supporting information

Supporting data to this article can be found online at https://doi.org/10.1016/j.apsb.2021.05.019.

References

1. DeAngelis LM. Brain tumors. *N Engl J Med* 2001;**344**:114–23.
2. Gao C, Liang J, Zhu Y, Ling C, Cheng Z, Li R, et al. Menthol-modified casein nanoparticles loading 10-hydroxycamptothecin for glioma targeting therapy. *Acta Pharm Sin B* 2019;**9**:843–57.

3. Salazar OM, Rubin P, Feldstein ML, Pizzutiello R. High dose radiation therapy in the treatment of malignant gliomas: final report. *Int J Radiat Oncol Biol Phys* 1979;**5**:1733−40.
4. Achrol AS, Rennert RC, Anders C, Soffietti R, Ahluwalia MS, Nayak L, et al. Brain metastases. *Nat Rev Dis Primers* 2019;**5**:5.
5. Eichler AF, Plotkin SR. Brain metastases. *Curr Treat Options Neurol* 2008;**10**:308−14.
6. Gallego Perez-Larraya J, Hildebrand J. Brain metastases. *Handb Clin Neurol* 2014;**121**:1143−57.
7. Lah TT, Novak M, Breznik B. Brain malignancies: glioblastoma and brain metastases. *Semin Canc Biol* 2020;**60**:262−73.
8. Wilson TG, Robinson T, MacFarlane C, Spencer T, Herbert C, Wade L, et al. Treating brain metastases from breast cancer: outcomes after stereotactic radiosurgery. *Clin Oncol (R Coll Radiol)* 2020;**32**:390−6.
9. Alnahhas I, Alsawas M, Rayi A, Palmer JD, Raval R, Ong S, et al. Characterizing benefit from temozolomide in MGMT promoter unmethylated and methylated glioblastoma: a systematic review and meta-analysis. *Neurooncol Adv* 2020;**2**:vdaa082.
10. Lauko A, Rauf Y, Ahluwalia MS. Medical management of brain metastases. *Neurooncol Adv* 2020;**2**:vdaa015.
11. Bocangel DB, Finkelstein S, Schold SC, Bhakat KK, Mitra S, Kokkinakis DM. Multifaceted resistance of gliomas to temozolomide. *Clin Cancer Res* 2002;**8**:2725−34.
12. Litak J, Mazurek M, Grochowski C, Kamieniak P, Rolinski J. PD-L1/PD-1 axis in glioblastoma multiforme. *Int J Mol Sci* 2019;**20**.
13. Wang X, Guo G, Guan H, Yu Y, Lu J, Yu J. Challenges and potential of PD-1/PD-L1 checkpoint blockade immunotherapy for glioblastoma. *J Exp Clin Cancer Res* 2019;**38**:87.
14. Khasraw M, Reardon DA, Weller M, Sampson JH. PD-1 Inhibitors: do they have a future in the treatment of glioblastoma?. *Clin Cancer Res* 2020;**26**:5287−96.
15. Yang T, Kong Z, Ma W. PD-1/PD-L1 immune checkpoint inhibitors in glioblastoma: clinical studies, challenges and potential. *Hum Vaccines Immunother* 2021;**17**:546−53.
16. Fresno Vara JA, Casado E, de Castro J, Cejas P, Belda-Iniesta C, Gonzalez-Baron M. PI3K/Akt signalling pathway and cancer. *Cancer Treat Rev* 2004;**30**:193−204.
17. Laplante M, Sabatini DM. mTOR signaling in growth control and disease. *Cell* 2012;**149**:274−93.
18. Wullschleger S, Loewith R, Hall MN. TOR signaling in growth and metabolism. *Cell* 2006;**124**:471−84.
19. Rathinaswamy MK, Burke JE. Class I phosphoinositide 3-kinase (PI3K) regulatory subunits and their roles in signaling and disease. *Adv Biol Regul* 2020;**75**:100657.
20. Prasad G, Sottero T, Yang X, Mueller S, James CD, Weiss WA, et al. Inhibition of PI3K/mTOR pathways in glioblastoma and implications for combination therapy with temozolomide. *Neuro Oncol* 2011;**13**:384−92.
21. Sami A, Karsy M. Targeting the PI3K/AKT/mTOR signaling pathway in glioblastoma: novel therapeutic agents and advances in understanding. *Tumour Biol* 2013;**34**:1991−2002.
22. Cully M, You H, Levine AJ, Mak TW. Beyond PTEN mutations: the PI3K pathway as an integrator of multiple inputs during tumorigenesis. *Nat Rev Cancer* 2006;**6**:184−92.
23. Samuels Y, Diaz Jr LA, Schmidt-Kittler O, Cummins JM, Delong L, Cheong I, et al. Mutant PIK3CA promotes cell growth and invasion of human cancer cells. *Cancer Cell* 2005;**7**:561−73.
24. Li X, Wu C, Chen N, Gu H, Yen A, Cao L, et al. PI3K/Akt/mTOR signaling pathway and targeted therapy for glioblastoma. *Oncotarget* 2016;**7**:33440−50.
25. Dreyling M, Morschhauser F, Bouabdallah K, Bron D, Cunningham D, Assouline SE, et al. Phase II study of copanlisib, a PI3K inhibitor, in relapsed or refractory, indolent or aggressive lymphoma. *Ann Oncol* 2017;**28**:2169−78.
26. Janku F, Yap TA, Meric-Bernstam F. Targeting the PI3K pathway in cancer: are we making headway?. *Nat Rev Clin Oncol* 2018;**15**:273−91.
27. Wilhoit T, Patrick JM, May MB. Alpelisib: a novel therapy for patients with PIK3CA-mutated metastatic breast cancer. *J Adv Pract Oncol* 2020;**11**:768−75.
28. Salphati L, Alicke B, Heffron TP, Shahidi-Latham S, Nishimura M, Cao T, et al. Brain distribution and efficacy of the brain penetrant PI3K inhibitor GDC-0084 in orthotopic mouse models of human glioblastoma. *Drug Metab Dispos* 2016;**44**:1881−9.
29. Maira SM, Stauffer F, Brueggen J, Furet P, Schnell C, Fritsch C, et al. Identification and characterization of NVP-BEZ235, a new orally available dual phosphatidylinositol 3-kinase/mammalian target of rapamycin inhibitor with potent *in vivo* antitumor activity. *Mol Cancer Therapeut* 2008;**7**:1851−63.
30. Papadopoulos KP, Tabernero J, Markman B, Patnaik A, Tolcher AW, Baselga J, et al. Phase I safety, pharmacokinetic, and pharmacodynamic study of SAR245409 (XL765), a novel, orally administered PI3K/mTOR inhibitor in patients with advanced solid tumors. *Clin Cancer Res* 2014;**20**:2445−56.
31. Zhou Q, Ji M, Zhou J, Jin J, Xue N, Chen J, et al. Poly(ADP-ribose) polymerases inhibitor, Zj6413, as a potential therapeutic agent against breast cancer. *Biochem Pharmacol* 2016;**107**:29−40.
32. Krishan A. Rapid flow cytofluorometric analysis of mammalian cell cycle by propidium iodide staining. *J Cell Biol* 1975;**66**:188−93.
33. Shaw LM. Tumor cell invasion assays. *Methods Mol Biol* 2005;**294**:97−105.
34. Lin S, Wang C, Ji M, Wu D, Lv Y, Zhang K, et al. Discovery and optimization of 2-amino-4-methylquinazoline derivatives as highly potent phosphatidylinositol 3-kinase inhibitors for cancer treatment. *J Med Chem* 2018;**61**:6087−109.
35. Zheng Q, Diao S, Wang Q, Zhu C, Sun X, Yin B, et al. IL-17A promotes cell migration and invasion of glioblastoma cells *via* activation of PI3K/AKT signalling pathway. *J Cell Mol Med* 2019;**23**:357−69.
36. He G, Zhang B, Zhang B, Qiao L, Tian Z, Zhai G, et al. Th17 cells and IL-17 are increased in patients with brain metastases from the primary lung cancer. *Chin J Lung Cancer* 2013;**16**:476−81.
37. Cantrell DA. Phosphoinositide 3-kinase signalling pathways. *J Cell Sci* 2001;**114**:1439−45.
38. Samuels Y, Velculescu VE. Oncogenic mutations of PIK3CA in human cancers. *Cell Cycle* 2004;**3**:1221−4.
39. Thorpe LM, Yuzugullu H, Zhao JJ. PI3K in cancer: divergent roles of isoforms, modes of activation and therapeutic targeting. *Nat Rev Cancer* 2015;**15**:7−24.
40. Miller BW, Przepiorka D, de Claro RA, Lee K, Nie L, Simpson N, et al. FDA approval: idelalisib monotherapy for the treatment of patients with follicular lymphoma and small lymphocytic lymphoma. *Clin Cancer Res* 2015;**21**:1525−9.
41. Wen PY, Cloughesy TF, Olivero AG, Morrissey KM, Wilson TR, Lu X, et al. First-in-human phase I study to evaluate the brain-penetrant PI3K/mTOR inhibitor GDC-0084 in patients with progressive or recurrent high-grade glioma. *Clin Cancer Res* 2020;**26**:1820−8.
42. Wen PY, Omuro A, Ahluwalia MS, Fathallah-Shaykh HM, Mohile N, Lager JJ, et al. Phase I dose-escalation study of the PI3K/mTOR inhibitor voxtalisib (SAR245409, XL765) plus temozolomide with or without radiotherapy in patients with high-grade glioma. *Neuro Oncol* 2015;**17**:1275−83.
43. Hainsworth JD, Becker KP, Mekhail T, Chowdhary SA, Eakle JF, Wright D, et al. Phase I/II study of bevacizumab with BKM120, an oral PI3K inhibitor, in patients with refractory solid tumors (phase I) and relapsed/refractory glioblastoma (phase II). *J Neuro Oncol* 2019;**144**:303−11.
44. Zhao W, Qiu Y, Kong D. Class I phosphatidylinositol 3-kinase inhibitors for cancer therapy. *Acta Pharm Sin B* 2017;**7**:27−37.
45. Gao N, Flynn DC, Zhang Z, Zhong XS, Walker V, Liu KJ, et al. G1 cell cycle progression and the expression of G1 cyclins are regulated by PI3K/AKT/mTOR/p70S6K1 signaling in human ovarian cancer cells. *Am J Physiol Cell Physiol* 2004;**287**:C281−91.
46. Hegedus B, Marga F, Jakab K, Sharpe-Timms KL, Forgacs G. The interplay of cell−cell and cell−matrix interactions in the invasive properties of brain tumors. *Biophys J* 2006;**91**:2708−16.

47. Wander SA, Zhao D, Besser AH, Hong F, Wei J, Ince TA, et al. PI3K/mTOR inhibition can impair tumor invasion and metastasis *in vivo* despite a lack of antiproliferative action *in vitro*: implications for targeted therapy. *Breast Cancer Res Treat* 2013;**138**:369−81.
48. Zhou H, Huang S. Role of mTOR signaling in tumor cell motility, invasion and metastasis. *Curr Protein Pept Sci* 2011;**12**:30−42.
49. McGeachy MJ, Cua DJ, Gaffen SL. The IL-17 family of cytokines in health and disease. *Immunity* 2019;**50**:892−906.
50. Zhang H, Chai W, Yang W, Han W, Mou W, Xi Y, et al. The increased IL-17-producing gammadelta T cells promote tumor cell proliferation and migration in neuroblastoma. *Clin Immunol* 2020; **211**:108343.
51. Wang B, Zhao CH, Sun G, Zhang ZW, Qian BM, Zhu YF, et al. IL-17 induces the proliferation and migration of glioma cells through the activation of PI3K/Akt1/NF-kappaB-p65. *Cancer Lett* 2019;**447**: 93−104.